Saturation effects in $K\alpha$ absorption spectroscopy of laser-produced plasmas

C. Chenais-Popovics, C. Fievet, J. P. Geindre, I. Matsushima,* and J. C. Gauthier
Laboratoire de Physique des Milieux Ionisés and Laboratoire d'Utilisation des Lasers Intenses, Ecole Polytechnique, 91128 Palaiseau CEDEX, France
(Received 10 April 1990)

In laser interaction, absorption of x rays by $K\alpha$ lines has been shown to be a powerful diagnostic of electronic temperature and integrated density in a dense absorbing plasma. Integrated densities measured in these experiments are lower than expected, especially in implosions where density is high. We present here an experiment and calculations that show that absorption saturates rapidly with increasing thicknesses of the absorber. An aluminum layer of variable thickness is heated by the soft x rays emitted by a samarium layer deposited on the laser-irradiated side of a planar target. We have measured the optical depth of the $K\alpha$ transitions of Al^{6+} to Al^{8+} ions as a function of the layer thickness. A strong nonlinear behavior is observed as predicted by the calculations. This type of saturation is explained by the high number of superimposed absorbing lines, and it is strongly dependent on the ratio between the linewidth and the instrumental resolution. Such a saturation effect is general for line absorption and does not appear on film when the instrumental broadening is larger than the line profile.

I. INTRODUCTION

$K\alpha$ spectroscopy has been used for a few years for integrated density and temperature measurements in dense plasmas of intermediate temperature (30–200 eV). It is a very powerful method that has been used in spherical implosions[1,2] as well as in planar experiments.[3–5]

Its main application is to diagnose regions that are too dense to emit x rays and that are out of the range of most diagnostics; in particular, emission spectroscopy or imaging. The purpose of the earliest experiments had been mainly the measurement of integrated densities in spherical geometry.[1,2,4,5] Later on, experimental and numerical studies were carried out in order to investigate more details of the physics subtending $K\alpha$ absorption.[6–8] Discrepancies between calculated and measured optical depths have been observed; the hypothesis of saturation effects has been put forward.[7] We present here an experiment and calculations that show this supposition to be correct. We show that density can be underestimated by using this diagnostic.

II. EXPERIMENTAL SETUP

One beam of the neodymium laser of the Laboratoire d'Utilisation des Lasers Intenses (LULI) has been focused on a multilayered target. The laser beam was frequency-quadrupled ($\lambda=0.26$ μm). Pulse duration was 500 ps, and energy was 15 J, giving intensities around 5×10^{14} W/cm^2 on target.

The target consisted of a 0.4-μm layer of samarium ($Z=62$) on the laser side, deposited onto a Mylar-aluminum-polyester multilayer. The aluminum layer thickness was varied from 0. 1 to 0.8 μm. Figure 1 is a schematic of the experimental setup which shows the different parts of the target. It explains the roles of sub-keV and keV x rays in the experiment. The samarium layer is heated by the laser. Its thickness has been adjusted from previous experiments to be of the same order as the ablated depth. It emits x rays around 1.5 keV in the spectral region where $K\alpha$ transitions are located. In this spectral region it plays the role of a backlighter. It emits also soft x rays in the 500-eV range[8] which are absorbed in the target and preheat it, thus creating a shallow temperature and density gradient.[9,10]

The 3.5-μm thickness of the Mylar that separates the Sm and Al layers has been chosen in order to have the highly absorbing C-like and B-like ions dominant in the aluminum layer.[6] The thickness of the plastic layer determines the temperature and ionization state of aluminum by fixing the distance between the emitter and absorber. The 2-μm-thick plastic layer at the rear of aluminum was chosen to reduce decompression of aluminum.

Figure 2 shows the temperature and density profiles obtained at the laser intensity maximum time in a simulation done with the radiative hydrocode XRAD.[9] Condi-

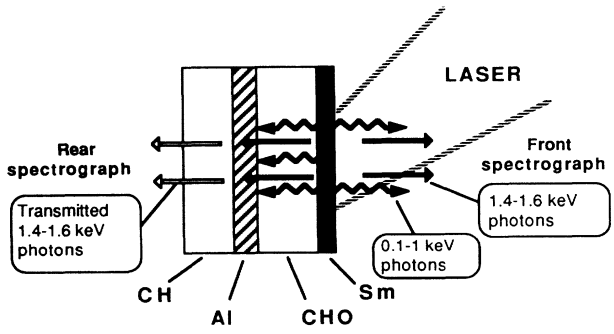

FIG. 1. Scheme of the targets used in the experiment. Arrows show the x rays and their role. The position of the crystal spectrographs is indicated.

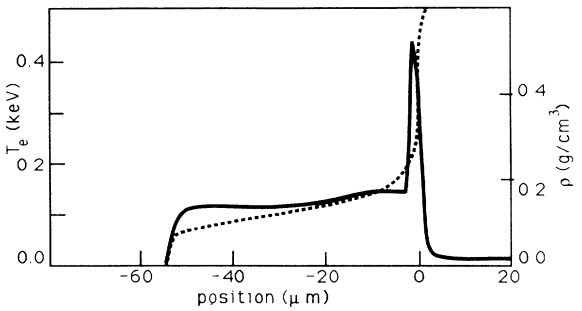

FIG. 2. XRAD radiative hydrocode simulation. Gradients of density (solid line) and temperature (dotted line) at laser maximum.

tions are close to the experimental ones (0.4 μm of Sm on top of 5 μm Mylar, 3×10^{14} W/cm^2 incident laser intensity at 0.26-μm wavelength). Aluminum is located in the shallow gradient where density is around 0.1–0.2 g/cm^3 and temperature is in the range of 80–100 eV during the samarium-emission probing time which is coincident with the laser intensity maximum.

Diagnostics consisted of a pinhole set at the front of the target which monitored the focal spot size and two time-integrated ammonic monophosphate (ADP) crystal spectrographs set in front and at the rear of the target. The front one recorded the emission Sm spectrum and the rear one measured the absorption of the Sm spectrum by aluminum $K\alpha$ transitions. We deduced the optical depth of the heated aluminum layer as a function of its thickness by subtracting the rear spectrum from the front one. We have done a careful wavelength calibration in order to superimpose exactly the front and rear spectra. In the adjustment of the intensities of the front and rear spectra, we multiplied the front spectrum by a scaling factor which takes into account self-absorption of the samarium layer.

III. NUMERICAL EVIDENCE OF $K\alpha$ ABSORPTION SATURATION

In a one-dimensional homogeneous nonemitting plasma, the radiation transfer equation simplifies to

$$I(\nu)=I_0(\nu)\exp\left[-\int_0^L \mu(\nu)\rho(x)dx\right]$$
$$=I_0(\nu)\exp[-\tau(\nu)]\ , \qquad (1)$$

where I_0 and I the incident and transmitted intensity at a given frequency ν. The absorption coefficient is μ (cm^2/g), $\rho(x)$ is the mass density at position x in the absorbing layer, L is the thickness of this layer, and τ is defined as its optical depth.

In Eq. (1), one can see that the space-averaged mass density of the absorbing layer $\langle \rho L \rangle$ is proportional to the frequency-integrated optical depth τ:

$$\langle \rho L \rangle \propto \int_{\Delta\nu} \tau(\nu)d\nu\ . \qquad (2)$$

Hence, absorption spectroscopy gives a measurement of $\tau(\nu)$ which is proportional to the averaged mass density $\langle \rho L \rangle$. Equation (1) shows that, when the absorption length increases, the transmitted intensity decreases exponentially. This decrease reaches a point where the transmitted intensity falls below the apparatus detection threshold. Absorption "saturates" when zero transmission is reached.

In the first section, we consider the simple case of an instrumentally broadened isolated line that illustrates very well the saturation mechanism. Then, we calculate the real case of $K\alpha$ transitions where a number of lines participate in the absorption for a given wavelength.

A. Saturation of an isolated spectra line

Figure 3 is a schematic of the transmission of a continuum spectrum through an absorbing plasma presenting a single absorption line in the considered spectral range. When the thickness of the absorbing layer is small the absorption line appears with its real profile in the continuum spectrum. When absorption depth increases, transmission falls to zero at the center of the line. If instrumental broadening is small compared to the absorption linewidth, one sees on the film that transmission goes to zero at the center of the line: absorption is then saturated.

Let us consider what happens when the instrumental broadening becomes greater than the absorption linewidth. The line appears as a convolution of the absorption line profile with the instrumental broadening given by

$$\frac{I_{\rm expt}(\nu)}{I_0}=\int_{-\infty}^{+\infty}\frac{I_{\rm theor}(\nu')}{I_0}g(\nu-\nu')d\nu'\ , \qquad (3)$$

where $I_{\rm theor}$ is given by Eq. (1) and g is the convolution factor. The absorption line profile appears in the absorption coefficient $\mu(\nu)$. We have assumed here that the backlighter source is uniform in the frequency space $[I_0(\nu)=I_0]$. This convolution leads to a transmission profile that does not reach zero even in the case of saturation (dashed line in Fig. 3). Therefore the saturation effect is not obvious in the experimental spectrum when

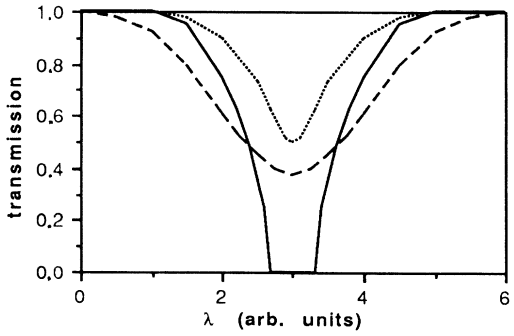

FIG. 3. Transmission of a continuum through an absorption line; principle of saturation. Dotted line, nonsaturated absorption line profile. Solid line, saturated absorption line without instrumental broadening; dashed line, instrumental broadened saturated line.

instrumental broadening is important.

For small absorbing-layer thickness, the optical depth integrated over frequencies increases linearly with the absorber thickness. When the saturation regime is reached, it still increases but much slower as transmission is saturated in the center of the line and increases in the wings.

B. $K\alpha$ absorption modeling

Transitions involved in $K\alpha$ absorption spectroscopy are $1s$-$2p$ transitions of F-like to He-like ionic stages that have a vacancy in the $2p$ shell.[6] They are shifted from the $1s$-$2p$ transitions of colder ions that are superimposed on the neutral $K\alpha$ line and several transitions are present for each ionic stage (2 to about 50 in aluminum have $\langle gf \rangle$ greater than 0.01). Many electrons are involved in the ground state of B- and C-like ions leading to a high number of $K\alpha$ transitions for these ion stages. The strongest lines coming from a given ion are grouped around the same frequency, and are superimposed, building a complex absorption structure. For the different ions, these structures are shifted from one another by approximately 30 eV, due to electron screening.

The radiative transfer equation can be generalized for the case of several transitions corresponding to different atomic levels of the same ion. The optical depth for ion stage i is given by

$$\tau(\nu,L)=\int_0^L k(n_i,\nu)dx \ , \tag{4}$$

where $n_i$is the ion stage i population. The absorption coefficient k, given here in cm^{-1}, is the sum of all the $1s$-$2p$ transitions which have a contribution at frequency ν. It is given by

$$k(n_i,\nu)=\frac{\pi e^2}{mc}\sum_{n,m} n_{i,n} f_{nm}\phi_{nm}(\nu) \ , \tag{5}$$

where e and m are the electron charge and mass, and c is the light speed. $n_{i,n}$ is the population of sublevel n of the ground state of ion i; f_{nm} and ϕ_{nm} are the oscillator strength and the absorption line profile of the $1s$-$2p$ transitions, which have a contribution at frequency ν.

As lines are grouped for a given ion stage, we can measure the space-integrated density of ion stage i, which is proportional to the integral of the optical depth over the frequency interval that covers all the lines corresponding to ion stage i:

$$\langle \rho L \rangle \propto \int_{\Delta\nu_i} \tau(\nu)d\nu \ . \tag{6}$$

In the experiments we measure an optical depth τ_{expt} modified by the convolution of the transmitted intensity by the instrumental profile. As convolution applies to transmitted intensity, the measured optical depth τ_{expt} is linked to the real optical depth τ_{theor} by

$$\tau_{\mathrm{expt}}(\nu)=-\ln\left[\int_{-\infty}^{+\infty}\exp[-\tau_{\mathrm{theor}}(\nu)]g(\nu-\nu')d\nu'\right] \tag{7}$$

We have calculated the optical depth τ_{theor} and its modified value τ_{expt} for the different ion stages of aluminum for a total mass density of 0.15 $\mathrm{g/cm}^3$, which corresponds to the conditions predicted by the radiative hydrocode XRAD simulation of the present experiment shown in Fig. 2. The electronic temperature is 80 eV, corresponding to the best fit of the experimental ionic distribution as deduced from $K\alpha$ absorption spectra.[9] We calculated the wavelengths and transition probabilities of all the strongest $1s$-$2p$ transitions of F to He-like ions with the code RELAC.[11–13] Populations of the levels were calculated assuming local thermodynamic equilibrium. A Voigt line profile was included for each individual transition. It included Doppler broadening that was of the order of 0.1 eV at 80 eV electron temperature. The natural width or the sum of the natural and autoionization widths has been included for each transition as the Lorentzian part of the Voigt profile. The natural width is around 0.1 eV, very comparable to the Doppler width. The autoionization width has been calculated with the RELAC code and is on the order of 1 eV. Stark broadening has been estimated[14,15] and is small for these low-quantum-number transitions. The backlighter source spectrum was assumed to be uniform in this calculation.

We have isolated each ionic stage, and calculated for each of them the optical depth $\tau_{\mathrm{theor}}(\nu)$ and the transmission of the line $I(\nu)/I_0$. Then, we have introduced the instrumental broadening of 2 eV and deduced the convolved transmission and the modified optical depth τ_{expt}. Figure 4 shows the results of this calculation for B-like aluminum, for a relatively large absorbing layer thickness (0.8 μm). In this calculation, the autoionization width was not included. In Fig. 4(a), one can see the high values of optical depth reached at the center of the lines (up to 60). The corresponding transmitted intensity goes to zero, as shown in Fig. 4(b). As explained in Sec. III A, this transmission, when convolved with the instrumental profile, no longer reaches zero, and the effect of saturation is masked [Fig. 4(c)]. Figure 4(d) shows the optical depth calculated from the broadened transmission. It stays at much lower values than the theoretical one [Fig. 4(a)]. The integral $\int \tau_{\mathrm{theor}}(\nu)d\nu$ reaches 72.2 as $\int \tau_{\mathrm{expt}}(\nu)d\nu$ does not go over 20.

We have performed this type of calculation for different thicknesses of the absorbing layer, including or not including the autoionization width. Results are shown for the B-like ion in Fig. 5, which represents the instrumentally broadened frequency integrated optical depth of B like ions as a function of the nonbroadened one. The solid line represents the linear case. With autoionization included (dashed line), i.e., when the linewidth is about half the instrumental width, absorption still saturates but much less than when only Doppler and natural widths are included (dotted line), i.e., when the linewidth is ten times smaller than the instrumental one. The nonlinear behavior of the integrated optical depth is obvious on this graph. Then the average mass density which is proportional to it will be underestimated. Moreover, one can see that saturation is highly dependent on the ratio between the width of the lines and instrumental broadening.

In Table I, we compare the values of linear and saturated integrated optical depths for all the different ion stages of aluminum (F-like to He-like). The calculation is

done for a 0.8-μm-thick absorbing layer. Table I gives ionic abundances and the energy range in which the integration is performed. It shows that only the dominant ions strongly saturate; the other ones remain very close to the linear regime. This difference in saturation for different ion stages changes the aspect of the absorption structures observed in the experiments by broadening their distribution. This broadening modified the inferred ionic distribution in a comparable way as temperature gradients would do.

IV. COMPARISON OF EXPERIMENTAL DATA WITH CALCULATIONS

In the experiment that we have performed, we have measured the optical depth of the absorbing layer for the dominant ion stages and compared them to the calculated ones. The 2-eV instrumental width measured on narrow lines of samarium was used in the calculations. Figure 6(a) shows the experimental optical depth as a function of photon energy. We see clearly absorption structures of F to Li-like ions. The distribution is characteristic of a temperature of 80 eV as shown by the theoretical spectrum in Fig. 6(b), obtained for a total density of 0.15 g/cm^3. We have restricted the spectral region of integration, as shown in Fig. 6(a) in order to increase the signal-to-noise ratio. We have restricted the analysis to the strongest lines (N-, C-, and B-like structures). Be-like ions have also a strong absorption, but we did not analyze them because they are superimposed on weak 1s-3p transitions.

Figure 7 shows the optical depths deduced from the

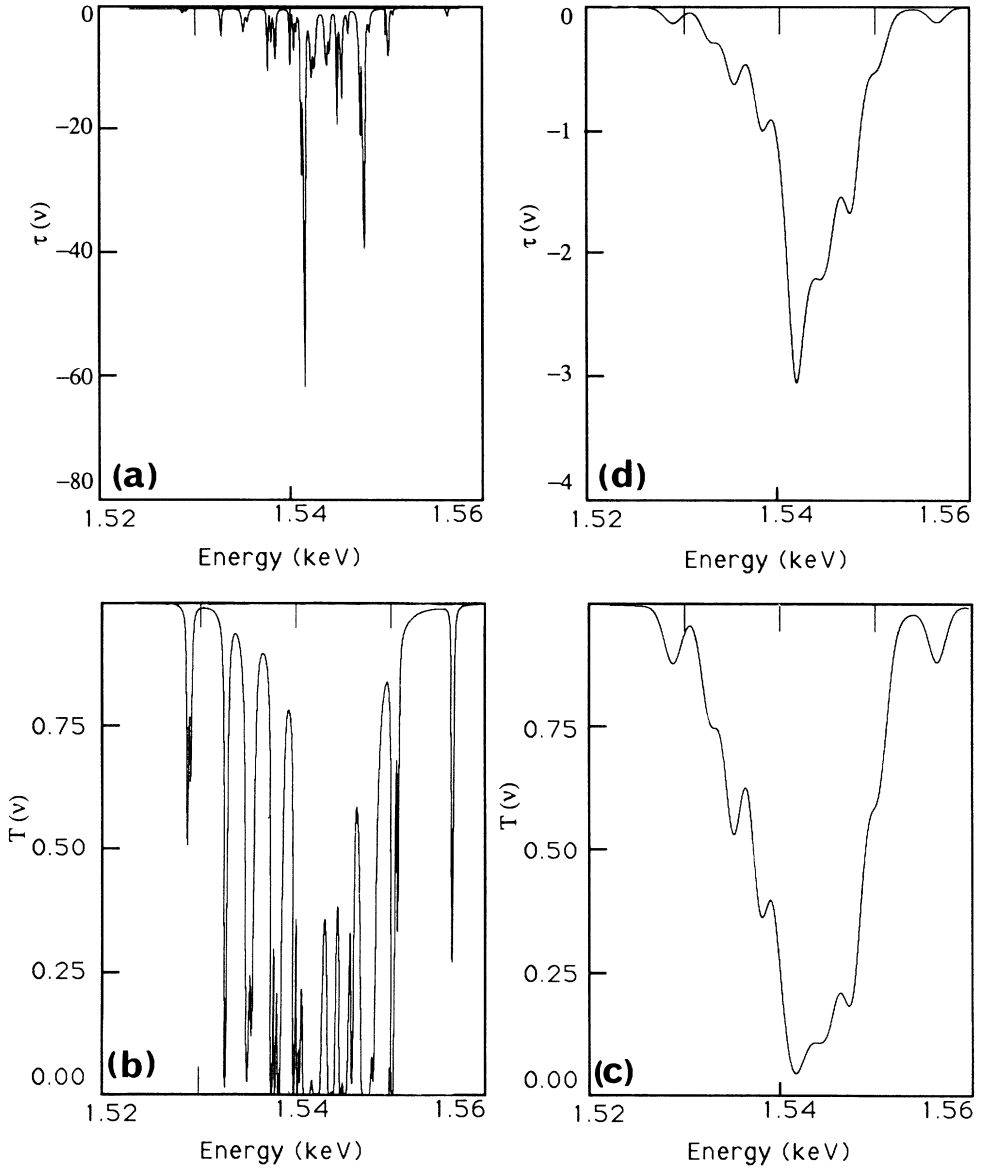

FIG. 4. Calculated transmission and optical depth of $K\alpha$ lines of Al^{8+} (B-like) with Doppler and natural widths. (a) optical depth without instrumental broadening; (b) transmission without instrumental broadening; (c) instrumental broadened transmission; and (d) optical depth deduced from the instrumental broadened transmission. ($\rho=0.15$ g/cm^3, $T_e=80$ eV; 2 eV instrumental broadening.)

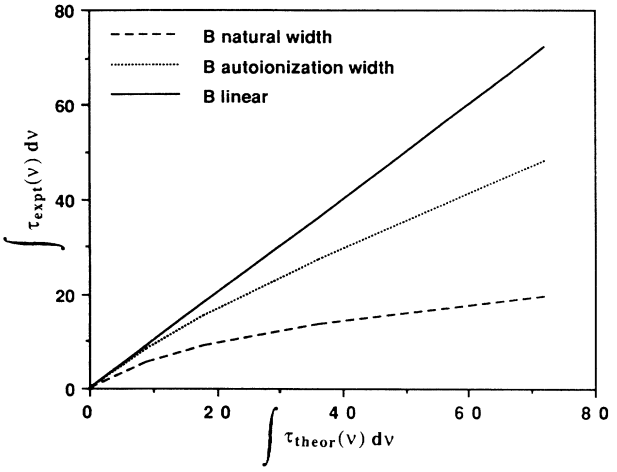

FIG. 5. Calculated frequency integrated optical depth of B-like $K\alpha$ transitions. On the y axis is represented the instrumentally broadened optical depth [integral of the curve drawn in Fig. 4(a)]; the x axis is the integral calculated before including instrumental broadening [from Fig. 4(d)]. Solid line, linear behavior, dotted line, autoionization included; dashed line, Doppler plus natural widths only.

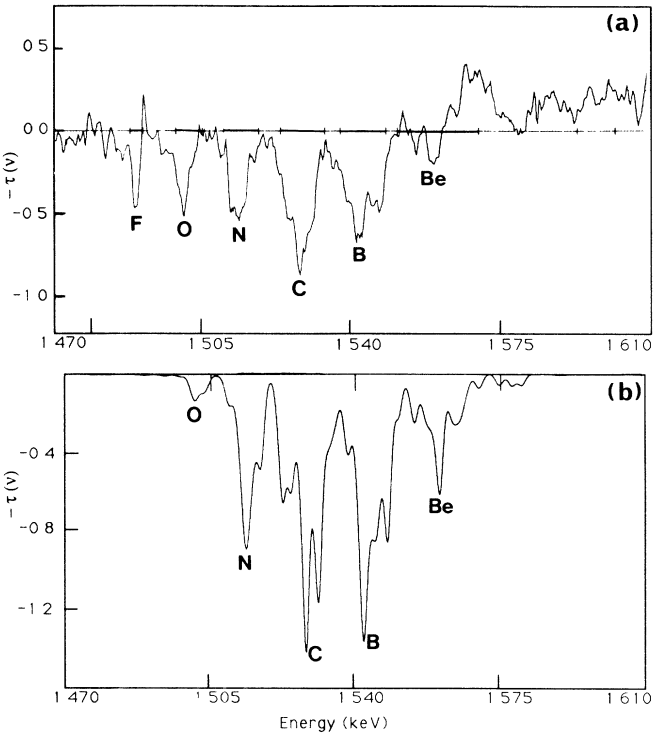

FIG. 6. Comparison of experimental and calculated optical depths of an aluminum layer. An 80-eV electronic temperature is deduced from this comparison. The heavy line on the x axis shows the energy range for the calculation of integrated optical depths.

measured spectra and the calculated ones. Experimental data show clearly a saturated behavior of the absorption. For only 0.1 μm of aluminum, all the ionic species absorb nearly linearly. For higher thicknesses, the absorption saturates for the dominant ion stages: B- and C-like experimental data (squares) are much lower than the linear behavior (solid lines). N-like data exhibit a low quasilinear absorption.

This is in agreement with a reduction of measured optical depths by saturation: C- and B-like ions have strong absorption and saturate, and N-like ions do not saturate because their population stays at a low level for the 80 eV electronic temperature reached in the absorbing layer. Dashed lines show the results of a calculation including autoionization in the absorption line profiles. It gives saturated values, but less saturated than the experimental data. A better fit of the experimental data is obtained when we included only Doppler and natural widths (dotted line).

We were expecting to have an agreement between experiment and the calculations that include autoionization. However, experiment gives much smaller optical depths, corresponding to a thickness three times smaller than the 0.8-μm-thick absorbing layer. We have investigated the possible reasons for this discrepancy. The first idea was that autoionization widths could be overestimated. We checked the autoionization rates obtained with previous calculations[16] dones for He- and Li-like ions. These calculations are in good agreement and have been used in comparisons of experiment and theory for Li-like

TABLE I. Integrated optical depths for a 0.8-μm-thick absorbing aluminum layer calculated with the following conditions: including Doppler and natural width, adding autoionization width, and linear calculation. Columns 2 and 3 give the integration energy range and the abundance of each ionic stage.

Al ion stage	Energy range (eV)	Ionization (%)	Doppler plus natural width	Auto-ionization width	Linear
F-like	1487.8–1490.9	6.010×10^{-4}	0.0003	0.0275	0.0275
O-like	1498.7–1504.9	1.369×10^{-2}	0.1720	0.3124	0.3380
N-like	1510.0–1518.3	0.1096	1.5124	1.8626	1.8837
C-like	1523.5–1534.0	0.3309	9.2694	16.5340	17.8120
B-like	1537.6–1548.2	0.3741	19.3430	43.3330	67.9400
Be-like	1551.0–1570.0	0.1510	26.6340	61.3230	116.8200
Li-like	1570.0–1593.5	1.944×10^{-2}	12.1610	19.7090	56.1200
He-like	1593.5–1602.4	5.917×10^{-4}	1.3050	1.4475	5.5321

dielectronic satellites without discrepancies.[17] We have no reason to think that these rates are incorrect. Also, it has been shown that autoionization does not give a symmetrical line profile, but a Fano profile.[18] We did not take this type of profile into account in the calculations, but such a difference is negligible in comparison to the factor of 10 on the Lorentzian linewidth needed for the best fit of the experiment.

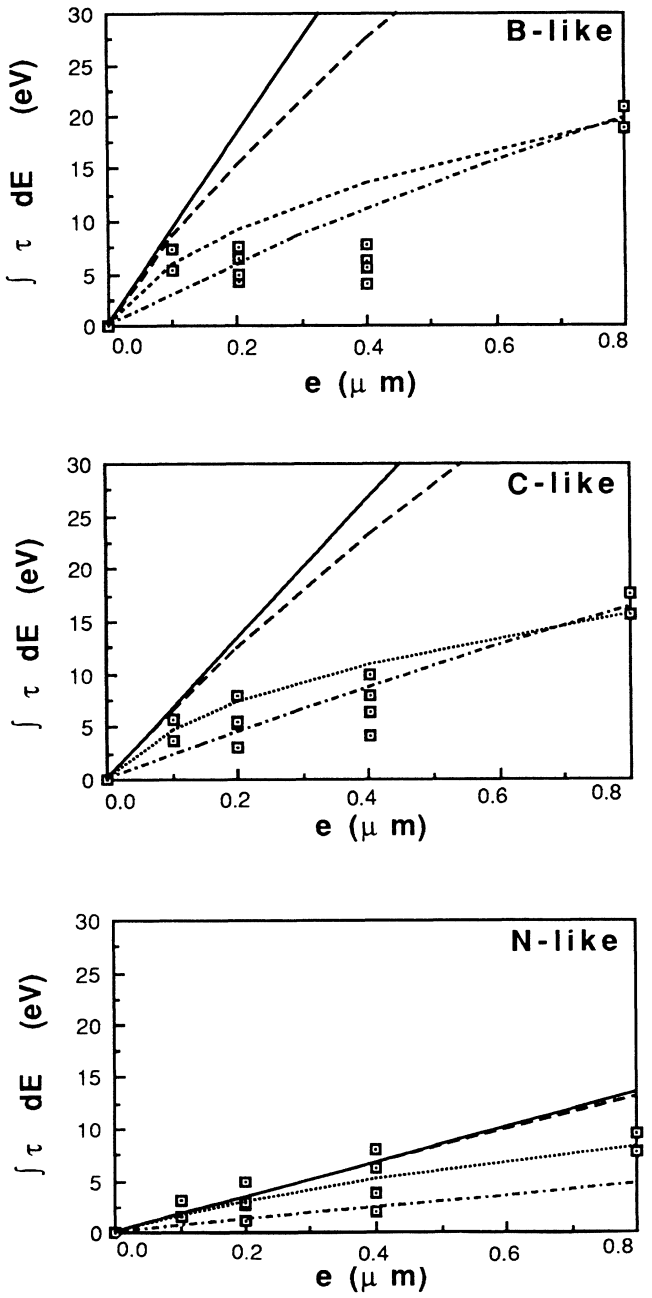

FIG. 7. Comparison of experimental and calculated frequency integrated optical depths of $K\alpha$ transitions of Al^{8+}, Al^{7+}, and Al^{6+} ions. (B-, C-, and N-like) as a function of Al layer thickness. Solid line, linear calculation; dashed line, autoionization width included; dotted line, autoionization width neglected; dash-dotted line, autoionization and a decompression factor of 3 included.

Another reason could come from lateral spreading of the target. Indeed, the target we used was a thin foil and two-dimensional (2D) effects were likely to occur. We expect that the target becomes thinner in the focal spot of the laser due to the ablation pressure. This decreases the thickness of the absorbing foil, and accordingly the optical depth is decreased. On a plot of measured optical depth as a function of absorbing layer thickness as in Fig. 7, this is equivalent to multiplying the abscissa by a decompression factor. Figure 7 shows that a best fit would require a factor of 3 decompression (dash-dotted line).

We have estimated the order of magnitude of this decompression following the conclusions obtained with a 2D Lagrangian hydrocode by Virmont and Faral, which describes the behavior of laser-irradiated thin foils.[19] Accordingly, we have assumed that during the laser pulse and the measurement duration, the target bends backwards like a circular arc in the 80-μm focal spot, the distance between the arc and the original target being the recoil of the target as calculated in the radiative hydrocode XRAD, i.e., 50 μm. Keeping the mass constant, the target gets thinner as it is stretched. This gives a factor-of-1.5 decompression as mass flows towards the sides of the target. The 1.5 decompression factor could be nearly sufficient to get an agreement between theory and experiment when taking into account the experimental error bars.

The last hypothesis we examined is linked to the backlighter source spectrum. First, as we mentioned in Sec. II, self-absorption of the samarium backlighter layer was taken into account by a multiplication factor on the front spectrum. In fact, reabsorption should be treated in a more complicated way if its role is important. This could be part of the reason for the discrepancy observed. Second, we suppose in the calculation that the backlighter source has a flat spectrum with no frequency dependence. It is obvious from the experiment that this was not the case. Samarium emission is composed of a number of resolved transitions and unresolved transition arrays. Then one can imagine that a thin absorption line could lay between emission lines. This could increase the transmitted intensity and decrease the apparent optical depth. The real transmission is then dependent on how the two arrays of absorption and emission transitions fit together. This effect is difficult to calculate, as the spectrum of samarium is too complex to be calculated in detail. Further work has to be done to check such an effect. However, one could expect an average in the fit as the high number of emission and absorption lines gives as much chance for an absorption line to spectrally coincide as for it not to coincide with an emission line. This average could validate the flat spectrum hypothesis that we have used.

V. CONCLUSION

The present calculations and experiment have evidenced and quantified saturation effects of $K\alpha$ absorption. The importance of this saturation is highly dependent on the ratio between instrumental and intrinsic linewidths. Even with only a factor of 2 between the in-

strumental and intrinsic linewidths saturation is non-negligible. Experimental data give a saturation higher than expected from the calculation. Further work on simple models describing the possible explanations for the discrepancy could help to understand the very low absorption observed in the experiment.

Using this $K\alpha$ absorption technique to measure space-integrated ion densities requires a good spectral resolution to avoid saturation, or a good knowledge of linewidths, in order to calculate properly the optical depths including saturation effects. The saturated behavior analyzed in this paper is a general feature of absorption spectroscopy and should be kept in mind in all the situations where the instrumental broadening is larger than the absorption line profile.

ACKNOWLEDGMENTS

The authors acknowledge the Laboratoire d'Utilisation des Lasers Intenses (LULI) staff for technical support on the laser. Films have been digitized on the Centre de Densitométrie et de Synthèse d'Images (CDSI) microdensitometer at the Paris–Sud University, and part of the calculations were performed on the Centre Inter Régional de Calcul Electronique (CIRCE) computer facilities at the Paris–Sud University.

*Permanent address: Electrotechnical Laboratory, 1-1-4, Umezono, Tsukuba, 305, Japan.

[1]A. Hauer, R. W. Cowan, B. Yaakobi, O. Barnouin, and R. Epstein, Phys. Rev. A **34**, 411 (1986).

[2]P. Audebert, D. K. Bradley, M. C. Richardson, R. Epstein, P. A. Jaanimagi, O. Barnouin, J. Delettrez, B. Yaakobi, F. J. Marshall, and B. L. Henke, SPIE Proc. **831**, 9 (1987).

[3]D. K. Bradley, J. D. Hares, and J. D. Kilkenny, Rutherford Appleton Laboratory Annual Report No. RL-83-043 (1983), p. 54.

[4]C. Chenais-Popovics, C. Fievet, J. P. Geindre, J. C. Gauthier, J. F. Wyart, and E. Luc-Koenig, SPIE Proc. **831**, 30 (1987).

[5]S. J. Davidson, J. M. Forster, C. C. Smith, K. A. Warburton, and S. J. Rose, Appl. Phys. Lett. **52**, 847 (1988).

[6]C. Chenais-Popovics, C. Fievet, J. P. Geindre, J. C. Gauthier, J. F. Wyart, and E. Luc-Koenig, Phys. Rev. A **40**, 3194 (1989).

[7]S. J. Davidson, C. L. S. Lewis, D. O'Neil, S. J. Rose, J. M. Forster, and C. C. Smith, in *Laser Interaction with Matter, European Conference on Laser Interaction with Matter Proceedings, Madrid, 1988,* edited by G. Velarde, E. Minguez, and J. M. Perlado (World Scientific, Singapore, 1989), p. 163.

[8]C. Chenais-Popovics, C. Fievet, J. P. Geindre, J. C. Gauthier, E. Luc-Koenig, J. F. Wyart, H. Pépin, and M. Chaker, SPIE Proc. **1140**, 581 (1989).

[9]J. C. Gauthier and J. P. Geindre, GRECO ILM Annual Report 1987, p. 176, available upon request from the authors.

[10]K. Eidmann, R. F. Schmalz, and R. Sigel, Phys. Fluids B **2**, 208 (1990), and references therein.

[11]E. Luc-Koenig, Physica **62**, 393 (1972).

[12]M. Klapisch, J. L. Schwob, B. S. Fraenkel, and J. Oreg, J. Opt. Soc. Am. **67**, 148 (1977).

[13]E. Luc-Koenig, M. Klapisch, and A. Bar-Shalom, unpublished computer code RELAC (1982).

[14]R. W. Lee, B. L. Whitten and R. E. Strout, J. Quant. Spectrosc. Radiat. Transfer **32**, 91 (1985).

[15]R. L. Kauffman, R. W. Lee, and K. Estabrook, Phys. Rev. A **35**, 4286 (1987).

[16]L. A. Vainstein and U. I. Safranova, At. Data Nucl. Data Tables **21**, 49 (1978).

[17]V. A. Boiko, A. Y. Faenov, and S. A. Pikuz, J. Quant. Spectrosc. Radiat. Transfer **19**, 11 (1978).

[18]R. P. Madden and K. Codling, Phys. Rev. Lett. **10**, 516 (1963).

[19]J. Virmont and B. Faral, GRECO ILM Annual Report 1985, p. 99, available upon request from the authors.